Numerical model for collisions in the drift approximation that reproduces classical and neoclassical transport

Qudsia Quraishi and Scott Robertson
Department of Physics, University of Colorado, Boulder, Colorado 80309-0390
(Received 11 February 2000)

A numerical method is described for including collisions in the drift approximation in a way that reproduces diffusion of the guiding center and of the drift orbit center. For untrapped particles, the method gives transport that agrees with classical values for mobility and diffusivity both parallel and perpendicular to the magnetic field. For trapped particles, the method correctly reproduces the neoclassical mobility and diffusivity. The model has been applied to the annular Penning trap in which a non-neutral plasma of electrons in a helical magnetic field makes collisions with neutral gas. The model shows that the transport makes a transition from neoclassical to classical values as the collision frequency goes from less than to greater than the axial bounce frequency.

PACS number(s): 02.60.−x, 52.65.−y, 52.25.Wz, 52.25.Fi

I. INTRODUCTION AND MOTIVATION

The drift approximation is advantageous to simulate particle motion in plasma confinement devices because it allows a much greater time step than can be used with the Lorentz equations of motion. The drift approximation is obtained by averaging the equations of motion over a period of gyration about the field lines. This averaging removes the period of gyration and the Larmor radius as time and distance scales that must be resolved. The drift approximation can be especially valuable for transport because the associated time scale is often many orders of magnitude longer than the gyration period. The averaging process, however, removes the details of particle motion that are needed to evaluate the guiding center displacements caused by collisions. We describe a method for putting collisions into the drift approximation in a way that correctly reproduces transport by both mobility and diffusion. We also show that the method correctly reproduces the neoclassical mobility and neoclassical diffusion [1,2] that apply to certain classes of confinement devices. Lastly, we apply the model to a simple experimental device having drift orbits with motion orthogonal to cylindrical flux surfaces. We show that a transition is made from neoclassical to classical transport as the collision frequency is changed from less than to greater than the frequency of the drift orbits.

Neoclassical transport occurs in omnigenous [3] confinement devices in which particles have drifts orthogonal to flux surfaces and the center of the drift orbit remains on a flux surface. A collision model for the drift approximation that reorients the velocity vector changes the width of the drift orbit and this causes the drift orbit center to diffuse in space [4,5]. This approach reproduces that part of neoclassical diffusion arising from diffusion of the drift orbit center; however, diffusion of the guiding center is lost. This is of little consequence when the drift orbit width greatly exceeds the Larmor radius. On the other hand, correct treatment of diffusion of the guiding center is essential for modeling the transition from neoclassical transport to classical transport that occurs when the collision frequency becomes sufficiently large to prevent the completion of drift orbits. For this reason the Lorentz equations of motion were used in the first numerical studies of the transition from neoclassical to classical transport in the tokamak [6].

The motivation for this work is to model confinement in an annular Penning trap [7], Fig. 1(a), in which the collisions are between electrons and neutral gas. The magnetic field

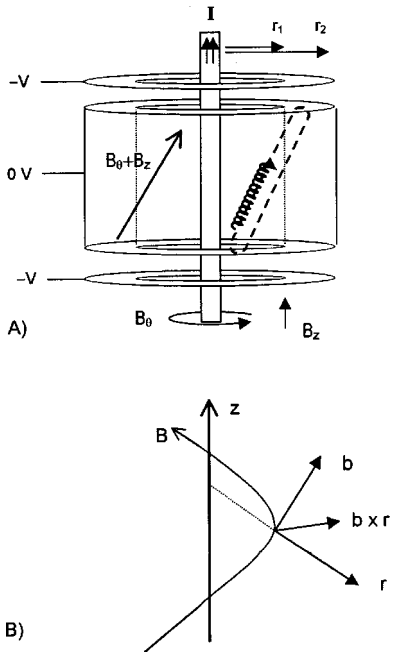

FIG. 1. (a) Schematic diagram of the annular Penning trap that is the motivation for the numerical model. There is an axial field B_z created by external coils and an azimuthal field B_θ created by an internal conductor with current I. The plasma is contained between concentric cylinders of radii r_1 and r_2 and loss along field lines is prevented by an electrostatic potential created by annular electrodes at the ends biased to a negative potential $-V$. An arrow shows the direction of the helical field. The spiral is the trajectory of an electron and the oval is the trajectory of its guiding center. (b) Local Cartesian coordinate system used in the analysis of particle collisions. The curved arrow is a helical field line.

 ©2000 The American Physical Society

geometry is cylindrical with magnetic fields B_θ and B_z that give straight cylindrical flux surfaces. Plasma of electrons is confined between two concentric cylinders that may be biased electrically to create a radial electric field E_r which drives transport by mobility. The electrons are confined axially by an electric field E_z at the ends of the device that accelerates particles toward the midplane. The axial field results in a bathtub-shaped potential well. The motion associated with the $\mathbf{E}_z \times \mathbf{B}_\theta$ drift in the end regions is radial and the particles drift a small distance radially while being reflected. This drift is in opposite directions at the two ends of the device and gives the bounce orbit of the guiding center a finite radial extent. The shape of the drift orbit is like that of a rubber band. This orbit is analogous to the bananalike drift orbit of the tokamak and results in transport being neoclassical [8].

In Sec. II, the numerical model for collisions in the drift approximation is presented. In Sec. III, we derive the classical and neoclassical transport coefficients for mobility and diffusion applicable to straight cylindrical flux surfaces having axially trapped particles. The model is applied in Sec. IV to the annular Penning trap with the collision frequency much greater than, equal to, or much less than the frequency associated with the drift orbits. In the limits of high and low collisionality, the calculated diffusivity agrees with the classical and neoclassical values, respectively.

II. THE COLLISION MODEL

A collision is modeled in the drift approximation in three steps: (1) the rest frame velocity of the colliding electron is redistributed randomly among the velocity components; (2) the displacement of the guiding center is found from the changes in velocity; and (3) the displacement across the electrostatic potential gradient is used to alter the particle kinetic energy so that the sum of kinetic and potential energies is conserved. We model electron-neutral collisions as hard-sphere collisions in which the electron velocity vector is reoriented randomly in the rest frame of the neutral gas. Low-energy collisions with monatomic gases are elastic collisions in which the length of the velocity vector is unchanged. The reorientation of the velocity vector, when averaged over many collisions, has the effect of removing the momentum associated with drift motion. This momentum loss is one of the driving forces for transport. The procedure described here could easily be modified for electron-ion collisions by selecting small random angular changes in the velocity vector [9].

In the drift approximation, there are gradient, curvature, and electric drifts that are the velocities perpendicular to the magnetic field. In addition, there is motion along the field line at a velocity $v_\parallel$. In our numerical model, these velocities are projected onto a cylindrical coordinate system and integrated using RK4 [10] to find the position of the guiding center as a function of time. The drift velocities are calculated at each position from the local fields and velocities. The parallel velocity is found by integration of the parallel acceleration. Thus, in the drift approximation, there are four variables found by RK4 on each time step rather than the six variables that would be necessary for the Lorentz equations of motion. The velocity $v_\perp$ in the plane perpendicular to B is found from the stored value of the magnetic moment of the particle and from the local value of the magnetic field. The time step is made sufficiently small to resolve the gradients in the electric and magnetic fields.

The analysis of collisions is simplified in a local Cartesian coordinate system, Fig. 1(b), at the particle location. This has one coordinate $\hat{\mathbf{e}}_b$ aligned with the magnetic field. A second coordinate $\hat{\mathbf{e}}_r$ is in the radial direction, which is perpendicular to the flux surfaces. This coordinate is the primary direction of the magnetic gradient, the electric field, and cross-field transport. The third coordinate, the $\hat{\mathbf{e}}_b \times \hat{\mathbf{e}}_r$ direction, is the direction of the dominant particle drifts. The unit vectors $\hat{\mathbf{e}}_r$, $\hat{\mathbf{e}}_{b\times r}$, and $\hat{\mathbf{e}}_b$ form a right-handed coordinate system.

The velocity vectors before and after the collision are found by the following procedure. The velocities used in the drift approximation, $v_\parallel$ and $v_\perp$, are the velocities parallel to $\hat{\mathbf{e}}_b$ and in the plane perpendicular to $\hat{\mathbf{e}}_b$, respectively. A random gyrophase θ is selected from 0 to 2π. A sine and a cosine are used to project $v_\perp$ onto the $\hat{\mathbf{e}}_r$ and $\hat{\mathbf{e}}_{b\times r}$ directions. The velocity in the $\hat{\mathbf{e}}_{b\times r}$ direction is added to the guiding center drifts in this direction to find the rest frame velocity of the particle. The squares of the rest frame velocity components are then summed to obtain the square of the magnitude of the velocity vector in the rest frame:

$$v_{\mathrm{tot}}^2 = (v_D + v_{\perp,1}\cos\theta)^2 + (v_{\perp,1}\sin\theta)^2 + v_{\parallel,1}^2 = v_D^2 + 2v_D v_{\perp,1}\cos\theta + v_{\perp,1}^2 + v_{\parallel,1}^2, \tag{1}$$

where v_D is the sum of the guiding center drifts in the $\hat{\mathbf{e}}_{b\times r}$ direction, $v_{\perp,1}$ is found from the local magnetic field and the stored value of the magnetic moment, the radial guiding center drifts are assumed negligible, and the subscript 1 refers to quantities before a collision. The cosine of the postcollision pitch angle, $\cos\alpha$, is selected randomly in the domain -1 to $+1$ and is used to project v_{tot} onto $\hat{\mathbf{e}}_b$:

$$v_{\parallel,2} = v_{\mathrm{tot}}\cos\alpha, \tag{2}$$

where the subscript 2 refers to quantities after a collision. This is done without a coordinate transformation between the drifting and rest frames because the drifts are orthogonal to this direction. The cosine is selected randomly rather than the angle so that all solid angles are given equal weighting. The remaining velocity is divided between the remaining two directions by selecting randomly an azimuthal angle β spanning 0 to 2π and using the sine and cosine:

$$v_{r,2} = v_{\mathrm{tot}}\sin\alpha\cos\beta, \tag{3}$$

$$v_{b\times r,2} = v_{\mathrm{tot}}\sin\alpha\sin\beta - v_D. \tag{4}$$

The azimuthal angle is not the pitch angle because the frame of reference is not the drifting frame. The guiding center drift has been subtracted to find $v_{b\times r,2}$ in the drifting frame. The sum of the squares of these velocities is the square of the new $v_\perp$:

$$v_{\perp,2}^2 = v_{r,2}^2 + v_{b\times r,2}^2, \tag{5}$$

where the radial guiding center drift has again been assumed negligible.

The guiding center displacement is calculated in the following way. First, the particle location is found by finding the vector $\mathbf{r}_1$ pointing from the stored guiding center location to the particle. The magnitude of this vector is the Larmor radius and its direction is opposite to the direction of the $\mathbf{v}\times\mathbf{B}$ acceleration of the magnetic field:

$$\mathbf{r}_1 = -m\mathbf{v}_1\times\mathbf{B}/qB^2, \tag{6}$$

where m is the electron mass and $q=-e$ is its charge. Second, this vector is evaluated again after the collision using the subsequent particle velocity $\mathbf{v}_2$. Third, this vector is subtracted from the particle location to yield the new position of the guiding center. These steps are combined to yield

$$\mathbf{x}_2 = \mathbf{x}_1 - m(\mathbf{v}_1-\mathbf{v}_2)\times\mathbf{B}/qB^2, \tag{7}$$

where $\mathbf{x}_1$ and $\mathbf{x}_2$ are the guiding center locations before and after the collision, respectively.

The components of the guiding center displacement are most easily evaluated in the plane perpendicular to $\hat{\mathbf{e}}_b$:

$$d_r = -m(v_{b\times r,1}-v_{b\times r,2})/qB, \tag{8}$$

$$d_{b\times r} = m(v_{r,1}-v_{r,2})/qB. \tag{9}$$

The second of these is projected onto the cylindrical rest frame coordinate system using

$$d_\theta = d_{b\times r}B_z/B, \tag{10}$$

$$d_z = -d_{b\times r}B_\theta/B. \tag{11}$$

At this point conservation of energy may have been violated because the guiding center has moved to a position where the electrostatic potential is different. The change in potential energy must be subtracted from the kinetic energy. In the case where the electric field is primarily radial, the potential energy before the collision is

$$\begin{aligned} W_p &= q\Phi(r_{\mathrm{GC}} - mv_{b\times r,1}/qB) \\ &= q\Phi[r_{\mathrm{GC}} - (mv_{\perp,1}/qB)\cos\theta], \end{aligned} \tag{12}$$

where $\Phi(r)$ is the electrostatic potential at the particle location, r_{GC} is the radial coordinate of the guiding center, θ is the gyrophase angle appearing in Eq. (1), and the potential has been assumed to be a function only of the radius. From Eqs. (1) and (12), the sum of the kinetic and potential energies is

$$W_{\mathrm{tot}} = W_p + \tfrac{1}{2}mv_{\mathrm{tot}}^2 = \tfrac{1}{2}m(v_D^2 + v_{\perp,1}^2 + v_{\parallel,1}^2) + q\Phi(r_{\mathrm{GC}}). \tag{13}$$

We have assumed that the gradient and curvature drifts are negligible so that $v_D = -E_r/B$, in which case the two terms with $\cos\theta$ cancel one another. A loss of potential energy arising from a displacement must be added to the kinetic energy through a revision in the value of $v_\perp$:

$$\begin{aligned} v_{\perp,2}^2 &= v_{\perp,2}^2 + 2(q/m)[\Phi(r_{\mathrm{GC}}) - \Phi(r_{\mathrm{GC}}+d_r)] \\ &\cong v_{\perp,2}^2 + 2d_r(q/m)E_r(r_{\mathrm{GC}}). \end{aligned} \tag{14}$$

Whether the potential or the field is used to find the correction is a choice that can be based upon which is most easily calculated. At the point where $v_{\perp,2}$ is found by taking a square root of the above expression, there is a small probability that the argument will be negative. This can be prevented with little loss in accuracy by setting negative values to zero. The new $v_{\perp,2}$ is used to revise the stored value of the magnetic moment.

Conservation of energy may also be used to find v_{tot} just before the collision. In this case Eq. (1) is replaced with

$$v_{\mathrm{tot}}^2 = 2[W_{\mathrm{tot}} - q\Phi(r_{\mathrm{GC}} - mv_{\perp,1}\cos\theta/qB)]/m. \tag{15}$$

For modeling problems having strong electric drifts or durations of 100 collision times or more, enforcement of energy conservation may be necessary because of inaccuracies inherent in the drift approximation. The use of Eq. (15) prevents conservation of energy from being used as a check on the accuracy of the computations.

III. TRANSPORT COEFFICIENTS FOR CYLINDRICAL GEOMETRY

The numerical model is tested by comparing the transport from the model with analytical values. For the annular Penning trap, the transport coefficients can be found most easily from a fluid approach. The fluid momentum equation for plasma of electrons is

$$nm\frac{d\mathbf{v}}{dt} = -\nabla P - nq\nabla\Phi + \mathbf{J}\times\mathbf{B}, \tag{16}$$

where P is the scalar electron pressure and $\mathbf{J}$ is the equilibrium current. The gradients are radial except in the end regions, which are ignored. The general solution for the equilibrium current is

$$\mathbf{J} = \mathbf{B}\times(\nabla P + nq\nabla\Phi)/B^2 + \lambda\mathbf{B}, \tag{17}$$

where λ is an adjustable constant. In the case of a long mean free path, the axial confinement results in there being no fluid z velocity and hence no J_z. This condition constrains the choice of λ and one finds that

$$J_\theta = \left(T\frac{dn}{dr} - nqE_r\right) \Big/ B_z, \tag{18}$$

where the gradient in the temperature (written in energy units) has been set to zero for simplicity. The equilibrium current is the sum of a diamagnetic drift part and an $\mathbf{E}\times\mathbf{B}$ drift part. Collisions with neutrals create a drag force on the equilibrium current:

$$F_\theta = -mv_\theta\nu = -mJ_\theta\nu/nq = -(m\nu/B_z nq)\left(T\frac{dn}{dr} - nqE_r\right) \tag{19}$$

where F_θ is the force per particle and ν is the electron-neutral momentum transfer collision frequency. The torque rF_θ changes the canonical angular momentum P_θ, and from this change the displacement causing transport can be found.

The canonical angular momentum may be averaged over the gyrophase and the axial bounce motion to obtain

$$P_\theta = r_0[mv_{D,\theta} + qA_\theta(r_0)] = r_0(mv_{D,\theta} + \tfrac{1}{2}qr_0B_z), \quad (20)$$

where r_0 is the radial location of the drift orbit center, $A_\theta(r)$ is the magnetic vector potential, $v_{D,\theta}$ is the θ component of the guiding center drift, and B_z is assumed to be spatially constant. The torque from collisions, rF_θ, changes the canonical momentum:

$$r_0F_\theta = \frac{dP_\theta}{dt} = \frac{d}{dt}[r_0(mv_{D,\theta} + \tfrac{1}{2}qr_0B_z)] \cong r_0qB_z\frac{dr_0}{dt}, \quad (21)$$

from which one finds the transport drift rate,

$$\frac{dr_0}{dt} = F_\theta/qB_z, \quad (22)$$

where we have used that $r_0 \gg |mv_{D,\theta}/qB_z|$. From the drag force on the equilibrium current, we obtain the particle flux Γ:

$$\Gamma = n\frac{dr_0}{dt} = -(m\nu T/q^2B_z^2)\frac{dn}{dr} + m\nu nE_r/qB_z^2$$

$$= -D_{\rm NC}\frac{dn}{dr} + n\mu_{\rm NC}E_r, \quad (23)$$

where

$$D_{\rm NC} = m\nu T/q^2B_z^2, \quad (24)$$

is the neoclassical diffusion coefficient. The neoclassical mobility coefficient

$$\mu_{\rm NC} = m\nu/qB_z^2 \quad (25)$$

relates the radial drift velocity to the radial electric field.

In the limit of short mean free path, local conditions rather than the end conditions determine the adjustable constant in Eq. (17). The current parallel to B is determined by an additional equation, a parallel Ohm's law, which relates the parallel current to the parallel electric field. There being no parallel electric field (except in the end regions), the parallel current is zero (rather than J_z) and $\lambda = 0$. In this case, one finds the classical values for mobility,

$$\mu_C = m\nu/qB^2, \quad (26)$$

and for diffusion,

$$D_C = m\nu T/q^2B^2 = \nu r_L^2, \quad (27)$$

where $r_L^2 = mT/q^2B^2$ is the square of the thermal Larmor radius.

The numerical model should also reproduce the coefficients for transport parallel to the field lines:

$$D_\parallel = T/m\nu, \quad (28)$$

$$\mu_\parallel = q/m\nu. \quad (29)$$

We return to the discussion of the numerical model and show that it correctly reproduces (1) the drift orbit width obtained from angular momentum conservation and (2) the neoclassical diffusion. The canonical momentum averaged over gyrophase alone is

$$P_\theta = r_{\rm GC}[m(v_{D,\theta} + v_\parallel B_\theta/B) + \tfrac{1}{2}qr_{\rm GC}B_z], \quad (30)$$

which in the absence of collisions is conserved. The velocity along the field line is reversed in the vicinity of the orbit tips and successive crossings of the midplane must be displaced radially by

$$2r_B = 2mv_{\parallel,0}B_\theta/qBB_z, \quad (31)$$

which is twice the drift orbit (banana) width r_B and $v_{\parallel,0}(B_\theta/B)$ is the azimuthal component of the parallel velocity evaluated at the midplane. From Eqs. (24) and (31), one finds

$$D_{\rm NC} = \nu(r_L^2 + r_{B,t}^2), \quad (32)$$

where $r_{B,t} = ({\rm mT})^{1/2}B_\theta/qBB_z$ is the thermal drift orbit width. This way of writing $D_{\rm NC}$ shows the separate contributions from the diffusion of the guiding center and the diffusion of the drift orbit center. The radial distance from the particle location to the flux surface with the drift orbit center is

$$\Delta r_{\rm GC} = mv_\parallel B_\theta/qBB_z. \quad (33)$$

The drift orbit width becomes the characteristic length for diffusion in the limit of small B_z in which $B_\theta \to B$.

It can be shown that the drift orbit width is correctly contained in the drift approximation by noting that $v_\parallel$ is changed by the time integral of the projection of the axial electric field onto the parallel direction:

$$-2mv_{\parallel,0} = q\int (B_z/B)E_z dt, \quad (34)$$

where the integral is taken along the orbit in the upper half plane. This time integral of E_z simultaneously results in a radial displacement from the radial component of the $\mathbf{E}\times\mathbf{B}$ drift:

$$2r_B = -\int (E_zB_\theta/B^2)dt = 2mv_{\parallel,0}(B_\theta/qBB_z), \quad (35)$$

where the previous equation has been used to eliminate the time integral. This displacement is the drift orbit width obtained from canonical momentum conservation.

A loss of momentum in a collision leads to neoclassical displacement of both the guiding center and the drift orbit center. The vector momentum removed by a collision may be decomposed into components in the $\hat{\mathbf{e}}_r$, $\hat{\mathbf{e}}_{b\times r}$, and $\hat{\mathbf{e}}_b$ directions. Loss of momentum in the $\hat{\mathbf{e}}_r$ direction results in a guiding center displacement in the $\hat{\mathbf{e}}_{b\times r}$ direction, and this transport is within, not across, the flux surfaces. Loss of momentum in the $\hat{\mathbf{e}}_{b\times r}$ direction results in transport in the $\hat{\mathbf{e}}_r$ direction through displacement of the guiding center. The relation of this momentum to the azimuthal momentum is $mv_\theta = mv_{b\times r}(B_z/B)$. The displacement of the guiding center from a momentum increment $m\Delta v_{b\times r}$, is

$$d_r = m\,\Delta v_{b\times r}/qB = m\,\Delta v_\theta/qB_z, \quad (36)$$

which is the neoclassical relationship between displacement and azimuthal momentum loss. Lastly, a momentum change in the $\hat{\mathbf{e}}_b$ direction results in no guiding center displacement; however, $v_\parallel$ is changed and there is a displacement of the drift orbit center relative to the guiding center. The relationship between this component of momentum and the azimuthal momentum is $mv_\theta = mv_\parallel(B_\theta/B)$. This relation placed into the expression for the distance from the guiding center to the drift orbit center, Eq. (33), yields a displacement of the orbit center

$$s_r = m\Delta v_\theta / qB_z , \tag{37}$$

which again is the neoclassical displacement. There is no need to add this displacement explicitly in the numerical model because the drift orbit is correctly reproduced in the drift approximation. Equations (36) and (37) show that a momentum change from a collision results in a displacement of the guiding center if in the $\hat{\mathbf{e}}_{b\times r}$ direction, a displacement of the drift orbit center if in the $\hat{\mathbf{e}}_b$ direction, and that in either case the displacement has the neoclassical relationship with loss of azimuthal momentum. The first equality in Eq. (36) is the classical result for the dependence of the displacement upon a change in momentum.

IV. APPLICATION TO THE ANNULAR PENNING TRAP

The numerical model is applied to the Penning trap by first finding the appropriate particle drifts. The electric drift is

$$\begin{aligned}\mathbf{v}_E &= (-E_z B_\theta \hat{\mathbf{e}}_r - E_r B_z \hat{\mathbf{e}}_\theta + E_r B_\theta \hat{\mathbf{e}}_z)/B^2 \\ &= -(E_z B_\theta / B^2)\hat{\mathbf{e}}_r - (E_r/B)\hat{\mathbf{e}}_{b\times r} .\end{aligned} \tag{38}$$

The gradient drift is

$$\begin{aligned}\mathbf{v}_{\nabla B} &= v_\perp^2(-B_z\hat{\mathbf{e}}_\theta + B_\theta \hat{\mathbf{e}}_z)B_\theta^2/2B^3 r\Omega \\ &= -(v_\perp^2 B_\theta^2/2B^2 r\Omega)\hat{\mathbf{e}}_{b\times r} ,\end{aligned} \tag{39}$$

where $\Omega = qB/m$ is the cyclotron frequency. The radius of curvature of a field line is $R_c = rB^2/B_\theta^2$ and this appears in the denominator. The inertial drift is

$$\begin{aligned}\mathbf{v}_1 &= (\mathbf{B}\times d\mathbf{v}_{\mathrm{GC}}/dt)/B\Omega \\ &= -v_{\theta_{\mathrm{GC}}}^2(\mathbf{B}\times\hat{\mathbf{e}}_r)/Br\Omega \\ &\approx -(v_\parallel B_\theta/B - E_r B_z/B^2)^2 \hat{\mathbf{e}}_{b\times r}/r\Omega \\ &= -(v_\parallel B_\theta/B - E_r B_z/B^2)^2 (B_z\hat{\mathbf{e}}_\theta - B_\theta\hat{\mathbf{e}}_z)/Br\Omega ,\end{aligned} \tag{40}$$

where dv_{GC}/dt is the centripetal acceleration $-v_{\theta_{\mathrm{GC}}}^2/r$ of the guiding center. This acceleration has contributions from $v_\parallel B_\theta/B$, the azimuthal component of the bounce motion, and from the azimuthal electric drift. These three drifts are summed in the numerical model to obtain the v_D used in evaluation of the total velocity.

The equation of motion parallel to the field is [11,12]

$$\begin{aligned}dv_\parallel/dt &= qE_\parallel/m + \mathbf{v}_E\cdot[(\mathbf{v}_E+\mathbf{v}_\parallel)\cdot\boldsymbol{\nabla}]\hat{\mathbf{e}}_b \\ &= (q/m)(E_z B_z/B) - (v_{E,\theta}+v_\parallel B_\theta/B)v_{E,r}B_\theta/rB \\ &\quad - v_{E,r}(v_{E,\theta}B_z^2 B_\theta + v_{E,z}B_z B_\theta^2)/rB^3 ,\end{aligned} \tag{41}$$

where $E_\parallel = E_z B_z/B$ is the projection onto the parallel direction of the electrostatic confining field at the ends of the trap. The terms after the first give the change in the parallel velocity due to the changing orientation of the parallel direction $\hat{\mathbf{e}}_b$. The azimuthal motion of the guiding center causes $\hat{\mathbf{e}}_b$ to rotate in the r-θ plane at the angular rate $(v_{E,\theta} + v_\parallel B_\theta/B)/r$. This change in $\hat{\mathbf{e}}_b$ at the particle location has a projection onto the radial electric drift $v_{E,r}$ occurring at the tips of the drift orbits. Additionally, the radial drift at the orbit tips carries the guiding center in the direction of the shear in the magnetic field. This causes $\hat{\mathbf{e}}_b$ to rotate in the θ-z plane and the rotation changes the projection of $\hat{\mathbf{e}}_b$ onto the other two components of v_E. The inclusion of these terms improves energy conservation from one side of the drift orbit to the other by an order of magnitude when there is an electric field applied to drive transport by mobility. There is no term from the $\boldsymbol{\nabla}\mathbf{B}$ force in this equation because there is no gradient of B in the parallel direction in the experiment being modeled. This term would be important for the tokamak, for example, where the $\boldsymbol{\nabla}\mathbf{B}$ force causes the reflection of particles at the drift orbit tips.

The assignment of initial particle velocities in the drift approximation is straightforward for the two degrees of freedom represented by $v_\perp$, but the assignment of initial velocities to $v_\parallel$ must be done with care. For axially confined particles on drift orbits, a particle with $v_\parallel = 0$ will be carried toward the drift orbit tips by the z component of the drifts, and there it will be reflected. This violates the requirement that the bounce motion should cease at zero parallel temperature. There is no bounce motion and the particle remains stationary in z when $v_\parallel$ has the value $v_{\parallel,D}$ to cancel the drifts in the z direction:

$$v_{\parallel,D} = -v_D(B/B_z) \cong -E_r B_\theta/BB_z , \tag{42}$$

where we have assumed that only the electric drift is significant. This velocity is added to the parallel initial velocities before they are assigned to the particles. This step may be omitted when the electric drift velocity is very much less than the thermal velocity.

The model was first applied to finding the drift orbits in the trap. Figure 2 shows drift orbits found from the Lorentz equations of motion and from the drift approximation. The experimental conditions were an inner cylinder radius of 25.4 mm, an outer cylinder radius of 50 mm, and cylinder lengths of 150 mm. The fields were $B_z = B_\theta = 2$ mT and E_r approximately 0.8 V/mm from a potential difference of 20 V applied to the outer cylinder with the inner cylinder at zero potential. To simplify testing the collision model, the electric field was specified rather than found from Poisson's equation. An electron was given an initial energy of 1 eV in each degree of freedom. The confining field E_z was modeled so that E_z and E_r together satisfied, approximately, Laplace's equation. The fields used in Fig. 2 were made lower than would be used in a laboratory experiment to better illustrate the cyclotron motion and the finite width of the drift orbit.

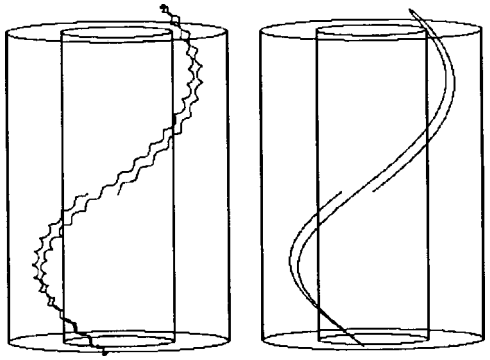

FIG. 2. A drift orbit plotted with the Lorentz equations of motion (left) and the drift approximation (right). The plots are made in the frame rotating with the $\mathbf{E}\times\mathbf{B}$ drift velocity.

The Lorentz equations of motion and the drift approximation give displacements at the end of one drift orbit that agree to within a few percent. The sources of drift E_r, $v_\perp$, and $v_\parallel$ were set to zero in pairs to verify that the drift arising from the remaining quantity alone was correctly reproduced. The failure of energy conservation at the end of one drift orbit is of order 10^{-5} when there are about 10 time steps in the steep-gradient region at each orbit tip where the confining field reverses $v_\parallel$. At the end of half a drift orbit, there are two sources of error arising from the differences in electric and magnetic fields from one side of the drift orbit to the other: (1) the change in the $\mathbf{E}\times\mathbf{B}$ drift velocity and (2) the change in $v_\perp$ arising from magnetic moment conservation. Motion along a field line into increasing B increases $v_\perp$ at the expense of $v_\parallel$. In the experiment being modeled, however, there is no gradient of B along B. The electrons cross the magnetic gradient because of the $\mathbf{E}\times\mathbf{B}$ drift occurring at the orbit tips and, in the drift approximation, this change in $v_\perp$ is not accompanied by an offsetting change in $v_\parallel$.

The numerical model was tested to confirm correct modeling of the transport described by the six coefficients $\mu_\parallel$, $D_\parallel$, μ_C, D_C, $\mu_{\rm NC}$, and $D_{\rm NC}$. For determination of $D_\parallel$ and D_C, the experiment was made infinitely long so that there were no drift orbits and no limit to the distance the particles could move in the z direction. This required simply setting to zero the confining field E_z. The experimental conditions were $B_z=5$ mT, $B_\theta=0$, $T=2$ eV (1 eV initially in each degree of freedom), $E_r=0$, $E_z=0$, and a time step giving 1 mm of displacement at the thermal velocity. The thermal velocity is 6×10^5 m/s and the gradient and inertial drifts are $\sim10^4$ m/s. The collision time was made 20 time steps and 256 particles were followed for 64 collision times. The squares of the displacements for the first 1000 collisions (the first four particles) are plotted in Fig. 3. A linear regression to all $\sim$16 000 collision points was compared with the analytical result for the random walk, $\langle r^2\rangle=2D_Ct$, and found to be lower by 6%. A similar plot was made for $\langle z^2\rangle$ as a function of time and the numerical result was 4% higher than the analytical result $\langle z^2\rangle=2D_\parallel t$. Repetitions of the tests yielded different percentages but in no case did the difference exceed 7%. These agreements were considered sufficiently good that the question of the differences being random or systematic was not pursued.

The mobility perpendicular to the field was examined by applying a radial electric field of -1000 V/m, giving v_D

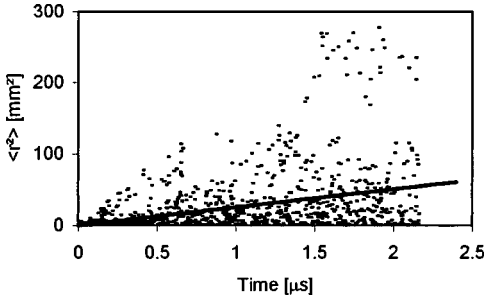

FIG. 3. A plot of the mean squared radial displacements of electrons as a function of time. Points are plotted at each collision and the line is a linear regression.

$=2\times10^5$ m/s, which is not sufficiently smaller than the thermal velocity for effects second order in E_r [in Eqs. (40) and (41)] to be ignored. Again 256 particles were followed for 64 collision times. The displacement by 64 collisions is of order 10 mm, resulting in a potential energy gain of order 10 V, which is sufficient to test energy conservation when there is Joule heating. A plot of $\sim$1000 positions as a function of time, Fig. 4, shows that, in addition to the mobility drift, there is significant diffusion that results in some particles returning to the origin. Conservation of energy, however, prevents diffusion beyond -3 mm, the point at which the initial 3 eV of kinetic energy is lost to potential energy. A linear regression to $\sim$16 000 points yields a mean displacement that is about 3% lower than the analytical value $\langle r\rangle=\mu_C E_r t$. A similar test was made with an axial field $E_z=-50$ V/m, and the mean axial displacement was compared with $\langle z\rangle=\mu_\parallel E_z t$. The numerical result was again about 3% lower than the analytical result. In all the tests without drift orbits, the sum of kinetic and potential energies was conserved to order 10^{-5} after 64 collisions.

The neoclassical diffusion was examined by applying an electric field to reflect particles at distances beyond ±75 mm. The axially trapped particles executed drift orbits like those shown in Fig. 2. The axial electric field strength at the ends was selected to reverse the axial motion in a distance of $\sim$5 mm so that spatial steps of order 1 mm were sufficient to resolve the potential gradient. The fields were set at $B_z=5$ mT and $B_\theta=10$ mT, which gives a thermal Larmor radius of 0.3 mm and a thermal drift orbit width of 0.6 mm. This separates the classical and neoclassical diffusivities by a

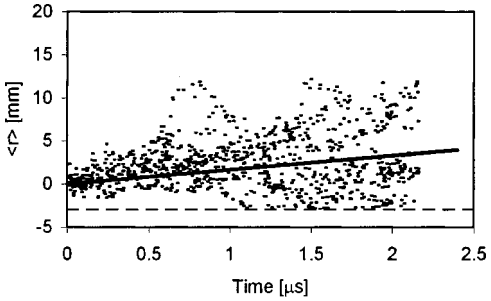

FIG. 4. A plot of the radial displacements of particles as a function of time with an applied radial electric field causing transport by mobility. Points are plotted at each collision and the line is a linear regression. The particle boundary at -3 mm is a consequence of conservation of energy.

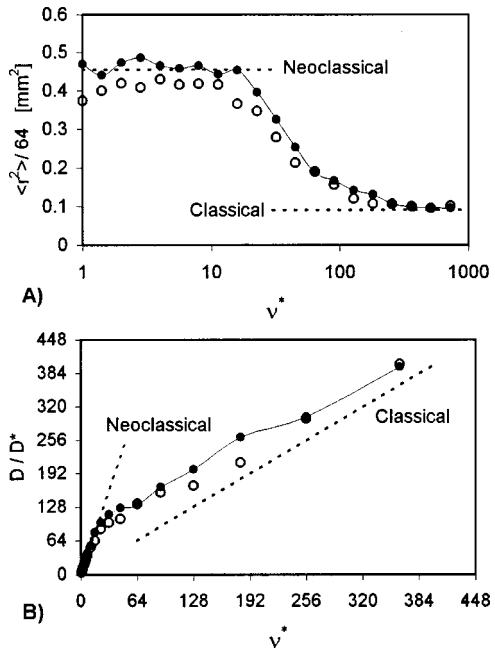

FIG. 5. (a) Mean square radial deviation of diffusing particles after 32 collisions as a function of the collisionality parameter ν^*. The upper dotted line is the expected value in the neoclassical regime and the lower dotted line is the expected value in the classical regime. The filled circles are with enforcement of energy conservation and the open circles are without. (b) A plot of diffusivity, normalized to the classical value at $\nu^*=1$, as a function of collisionality. The points are spaced logarithmically by half powers of 2.

factor of 5. The paths of 1000 particles were followed for 32 collisions, which gives a mean squared radial deviation of $64r_L^2$ for classical diffusion and $64(r_L^2+r_{B,t}^2)$ for neoclassical diffusion. The collision frequency was changed in logarithmic steps from less than to greater than the drift orbit frequency ω_B, defined as 2π divided by the drift orbit bounce time. The mean square deviations are plotted in Fig. 5(a) as a function of $\nu^*=\nu/\omega_B$. The filled circles are with enforcement of energy conservation, Eq. (15), and the closed circles are without, Eq. (1). At low collisionality, $\nu^*<10$, the diffusion is near the neoclassical value and at high collisionality $\nu^*>100$, the diffusion is near the classical value. The diffusivity is plotted as a function of ν^* in Fig. 5(b). The diffusivity has been divided by $D^*=\omega_B r_L^2$ so that the slope of the plot is unity at high collisionality and $1+(r_{B,t}/r_L)^2=5$ at low collisionality. The electrons were initially distributed randomly along the length of the device at a radius of 40 mm. Examination of the data showed that, at intermediate collisionality (the plateau), the particles initially near the orbit tips diffused the greatest distances. The energies of the electrons wandered by about $\sim$0.1 eV during the tests without energy conservation except for the longest tests ($\nu^*<8$), where the mean energy was reduced by $\sim$0.5 eV, causing a systematic reduction in the diffusivity. The average of the mean square deviations obtained at ν^* values spanning 1 to 8 is 1.02 of the neoclassical value. An average of the mean square deviations for $\nu^*=512$ and 724 is 1.06 of the classical value.

The usual plateau of the neoclassical theory for tokamaks connects neoclassical diffusion with Pfirsch-Schlüter diffusion rather than with simple classical diffusion [6,13]. Tokamak transport arises from collisions of both passing particles and trapped particles and from collisions causing transitions of particles from one class to the other. Thus, transport in the annular trap is less complicated than that in the tokamak. In the simulations, all of the particles have the same collision frequency, which would not be the case in laboratory plasma.

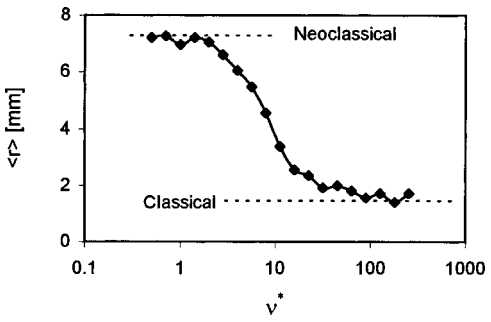

FIG. 6. Mean radial displacement as a function of collisionality for 1000 particles after 32 collisions with a radial electric field of -1000 V/m. The upper dotted line is the value based upon the neoclassical mobility and the lower line is the value based upon the classical mobility.

The neoclassical perpendicular mobility was examined with the same parameters as the classical perpendicular mobility except that the axial confining field was applied at the ends to create drift orbits. The mobility resulted in particles moving preferentially ''downhill'' in the electrostatic potential as a result of collisions. The particles gained 1 eV of energy per mm of displacement. The energy error accumulated after 32 collisions became comparable, for those particles moving several centimeters, to the initial kinetic energy. The errors were much smaller when there was no electric field. To eliminate the error, the program was modified so that energy conservation, Eq. (15), was used to find the magnitude of the velocity before the collision. Plotted in Fig. 6 is the mean drift distance for 1000 particles after 32 collision times as a function of ν^*. Also shown are the mean displacements calculated from the classical and neoclassical mobilities. The calculated displacement is approximately the neoclassical value for $\nu^*<2$ and is approximately the classical value for $\nu^*>90$. The average of the mobility values for $\nu^*=0.5$, 0.7, 1, and 1.4 is 2% below the neoclassical value and the average for $\nu^*=90$, 128, 181, and 256 is 10% higher than the classical value. In computations in which energy conservation was not enforced, the energy error did not perceptibly change the mobility; however, the diffusivity was increased. This difference in sensitivity to energy error arises because the diffusivity is dependent upon the particle energies and the mobility is not.

V. SUMMARY AND CONCLUSION

A method has been described for simulating with the drift approximation plasma transport arising from collisions of electrons with neutral gas. At the time of a collision, a random gyrophase is selected and used to construct a velocity vector. This vector is repointed randomly in the rest frame, the displacement of the guiding center is found, the kinetic energy is corrected for the change in the electrostatic potential energy arising from the displacement, and integration of

the guiding center equations of motion is resumed. The method reproduces, to within about 5%, classical values for mobility and diffusion both perpendicular and parallel to the magnetic field. Neoclassical transport is reproduced for particles trapped electrostatically in the helical magnetic field of the annular Penning trap. The method finds the dependence of the diffusivity upon collisionality in the ''plateau'' region in which the collision frequency goes from less than to greater than the frequency of the drift orbit. The transition from neoclassical to classical behavior begins when the collision frequency is about 10 times the drift orbit frequency (in radians per second) and is completed when the collision frequency is about 100 times the drift orbit frequency.

ACKNOWLEDGMENTS

The authors thank Professor John Cary and Professor Scott Parker for helpful discussions.

[1] B. B. Kadomtsev and O. P. Pogutse, Nucl. Fusion **11**, 67 (1971).
[2] F. L. Hinton and R. D. Hazeltine, Rev. Mod. Phys. **48**, 239 (1976).
[3] L. S. Hall and B. McNamara, Phys. Fluids **18**, 552 (1975).
[4] A. H. Boozer and G. Kuo-Petravic, Phys. Fluids **24**, 51 (1981).
[5] R. E. Potok, P. A. Politzer, and L. M. Lidsky, Phys. Rev. Lett. **45**, 1328 (1980).
[6] K. T. Tsang, Y. Matsuda, and H. Okuda, Phys. Fluids **18**, 1282 (1975).
[7] S. Robertson and B. Walch, Rev. Sci. Instrum. **70**, 2993 (1999); J. Kline, S. Robertson, and B. Walch, in *Non-Neutral Plasma Physics III*, edited by J. J. Bollinger, R. L. Spencer, and R. C. Davidson, AIP Conf. Proc. No. 498 (AIP, New York, 1999), p. 290.
[8] S. Robertson, Phys. Plasmas **4**, 2760 (1997).
[9] R. Shanny, J. M. Dawson, and J. M. Greene, Phys. Fluids **10**, 1281 (1967).
[10] W. H. Press, B. P. Flannery, S. A. Teukolsky, and W. T. Vetterling, *Numerical Recipes, the Art of Scientific Computing* (Cambridge University Press, Cambridge, 1986), Chap. 15.
[11] G. Schmidt, *Physics of High Temperature Plasmas* (Academic, New York, 1979), Chap. 2.
[12] K. Miyamoto, *Physics for Nuclear Fusion* (MIT Press, Cambridge, MA, 1979), Chap. 3.
[13] See, for example, J. Wesson, *Tokamaks* (Clarendon, Oxford, 1987), Chap. 4.